A Bio-inspired Embedded Vision System for Autonomous Micro-robots: the LGMD Case

Cheng Hu, Farshad Arvin, *Member, IEEE,* Caihua Xiong, *Member, IEEE,* and Shigang Yue, *Member, IEEE*

***Abstract*—In this paper, we present a new bio-inspired vision system embedded for micro-robots. The vision system takes inspiration from locusts in detecting fast approaching objects. Neurophysiological research suggested that locusts use a wide-field visual neuron called lobula giant movement detector (LGMD) to respond to imminent collisions. In this work, we present the implementation of the selected neuron model by a low-cost ARM processor as part of a composite vision module. As the first embedded LGMD vision module fits to a micro-robot, the developed system performs all image acquisition and processing independently. The vision module is placed on top of a micro-robot to initiate obstacle avoidance behaviour autonomously. Both simulation and real-world experiments were carried out to test the reliability and robustness of the vision system. The results of the experiments with different scenarios demonstrated the potential of the bio-inspired vision system as a low-cost embedded module for autonomous robots.**

***Index Terms*—Bio-inspired, LGMD, Collision avoidance, Embedded system, Autonomous robot, Low-cost.**

I. Introduction

THE ability to avoid a collision is an important issue for the autonomous mobile robots. There are different sensory systems which are used for collision avoidance such as ultrasonic [1], infra-red [2], [3] , laser [4], radar [5] and vision system [6]. However, it is still not an easy task for mobile robots to run autonomously in complex environments without human intervention. Amongst these modalities, vision often provide rich cues to interpret the real world as demonstrated in many animal species. In building artificial vision systems, one of the greatest challenges is to understand and deal with the dynamic scenes [7] with complex background, moving objects and/or rapidly changing ambient light. Fast and reliable methods to address these problems are needed.

Nature demonstrates variety of the successful visual methods in collision avoidance [8]. For example, in locusts, the ability to detect approaching objects is important to avoid collision in dense swarm or escape from predators [9]. It has been identified that there is a wide-field visual neuron in the lobula layer of the locust nervous system called the Lobula Giant Movement Detector (LGMD) [10] which plays a critical role for the ability of collision detection and avoidance. As the results of millions years of evolution, the vision-based collision avoidance systems in animals, such as LGMD, are both reliable and efficient in coping with dynamic environments [11]–[13]. Therefore, it can be a feasible approach if we take inspiration from nature and apply it on autonomous mobile robots.

The LGMD neuron in locust has an unique character responding selectively to looming objects [14]. It generates high frequency spikes to an object approaches in a direct collision course rapidly [15]. LGMD is tightly tuned to respond to objects approaching in a direct collision course [16], however it produces little or no response to receding objects [15], [17]. Compared to the vision processing systems in large mammals like humans, LGMD uses relatively smaller number of neurons and simpler structures to perform collision detection function. All these characteristics make LGMD an ideal model for developing a specialised, fast and low-cost vision system for autonomous collision avoidance [18]–[20] .

As an early work on LGMD modelling, a functional neural network based on the LGMD's input circuitry was developed by Rind and Bramwell [21]. This neural network showed the same selectivity as the LGMD neuron for approaching objects and responded best to the objects approaching on collision rather than near-miss trajectories. This neural network has also been used to mediate collision avoidance in a real-world environment by incorporating it into the control structure of a miniature robot [18], [22].

In the previous LGMD based collision avoidance researches [18]–[20], robots only serve for the image acquisition and the motion control due to limited computing power and hardware resources on board. The major LGMD processing tasks were completed by the models written with PC-based software such as MATLAB (Mathworks, USA). Collision avoidance was conducted upon receiving the computation results transferred from the host PC via cables or wireless signals [19], [23]. The whole system is cumbersome and complicated to autonomous miniature multi-robot systems such as swarm robotics scenarios [24]. Therefore, a much more compacted implementation of a LGMD model in one miniaturized module for autonomous collision detection is badly needed. The reduction in size will not only make it easy to integrate into micro-robots, but will also lead to low-cost and low power consumption.

This work was supported by EU FP7 projects LIVCODE (295151), HAZCEPT (318907), HORIZON 2020 project STEP2DYNA (691154), National Natural Science Foundation of China (51335004) and 973 National Basic Research Program of China (2011CB013301).

Cheng Hu and Shigang Yue are with the Computational Intelligence Lab (CIL), School of Computer Science, University of Lincoln, Lincoln LN6 7TS UK (email: chu@lincoln.ac.uk; syue@lincoln.ac.uk, yue.lincoln@gmail.com, corresponding author).

Farshad Arvin is with School of Electrical and Electronic Engineering, The University of Manchester, Manchester, M13 9PL, UK (email: farshad.arvin@manchester.ac.uk).

Caihua Xiong is with School of Mechanical Science and Engineering, Huazhong University of Science and Technology, Wuhan, 432700, China (email: chxiong@hust.edu.cn).

Part of this paper was presented on 2014 Joint IEEE International Conferences on Development and Learning and Epigenetic Robotics (ICDL-Epirob), Italy.

In this research, we aim to push the realization and application of bio-inspired visual systems, LGMD in this case, one step further, by integrating the collision detection and avoidance model and all functionalities to one compact board as a "plug and play" module to micro-robots. In order to achieve this, the LGMD model was rewritten to fit to an embedded vision module featuring by an ARM® micro-controller chip which serves as the main processor and also acquires video sequence from a tiny CMOS camera. This vision module enables a low-cost micro-robot, *Colias* [25], to demonstrate autonomous collision detection and avoidance behaviour, which was tested in various experiments with different environmental configurations.

The rest of this paper is organised as follows. In section II, we give an overview of related work. In section III, we talk about the robot's system design. Section IV describes the proposed LGMD model, which also explains its realization on an embedded processor. The experiments and results are illustrated in Section V. Following that, in Section VI, we further discuss about the proposed system and future research directions.

II. Related Work

A. Traditional Vision Based Collision Detection Methods

Vision-based collision detection is widely used in robotics [26], [27]. For example, Suman et al. [28] proposed a monocular obstacle detection and avoidance method for unmanned aerial vehicle (UAV). They used mathematical model to estimate the relative distance from the UAV's camera to an obstacle by detecting the feature points in the UAV's field of view, which is not an on-board system.

Yaghmaie et al. [29] proposed a novel method for robots to navigate in dynamic environments called Escaping Algorithm which is based on force field method which belongs to the family of Simultaneous Localization And Mapping (SLAM). In their algorithm, the movement of dynamic obstacles is predicted by Kalman filter for collision detection combined with potential field approach. The method was tested on simulations then implemented by a mobile robot platform, however, the computing task was done on a PC with Intel® i5 processor.

Traditional visual based collision detection methods need to process massive volume of images in real time or need a real-world model created in advance, which is either difficult to be completed on-board for a micro-robot with limited resources or hardly able to cope with dynamic environments.

B. Bio-inspired collision detection methods

There are also several bio-inspired collision avoidance and navigation methods, most of which are based on elementary motion detector (EMD), for example Zhang et al. [30], Badia et al. [31] and Franceschini et al. [32]. However, in many cases, EMD based methods could be difficult to apply due to its inherent character - the performance is strictly restricted within certain visual speeds.

LGMD based methods, on the other hand, can cope with most of the upcoming collisions, regardless of the visual speed. Blanchard et at. [18] was the first to bring LGMD based neuron networks into robots for real-time collision detection and tested it with Khepera I robots. Badia et al. [23] proposed one form of LGMD based collision detection model and tested it on a high-speed robot "Strider" with a wireless camera to capture and transmit images to PC for processing. Silva et al. [33] proposed another modified LGMD model which combined two previous works from [19] and [34] for more robust collision detection, which focused more on modelling instead of embedded system development.

There has been effort on implementing bio-inspired method in VLSI chips like FPGA, for example, Meng et al. [34] added additional cell to detect the movement in depth, Harrison [35] proposed an Analog IC for visual collision detection based on EMD, and Okuno and Yagi [36] implemented mixed analog-digital integrated circuits with FPGA. However, these attempts are not suitable for micro and mini robots, either because of the large size or the high power consumption of the FPGA circuits.

III. ROBOT SYSTEM FORMULATION

The micro-robot system realisation contains mainly two parts: *Colias* [25] swarm robotic platform and the developed vision processing module. Fig.1(a) shows the Colias robot platform.

A. Robot Platform

We have chosen Colias as our testing platform for the following reasons. First, it is a light weight robot that reacts to motion commands fast. Second, Colias is one of the smallest and cheapest micro-robots in the field, so that multiple robots could be put in one small arena to test both the individual and collective behaviours.

Colias employs a circular platform with a diameter of 4 cm with two independent boards: the upper board and the lower board. The upper board is developed for inter-robot communication and swarm robotic scenarios [37]. In the current work, we removed the upper board and only the lower board of Colias was deployed. Fig. 1(b) shows the basic architecture of Colias robot. The marked block is the lower board of Colias which is used as the micro-robot platform.

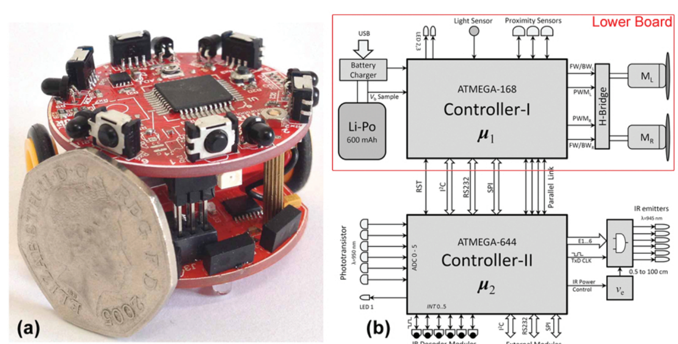

Fig. 1. (a) Colias robot platform and (b) basic architecture of Colias. The bottom board, which is marked within a red rectangle in (b), is deployed in this study.

The Colias platform provides motion, basic short-range proximity sensors and power management. It uses an ATMEL AVR 8-bit micro-controller with 8 MHz internal clock source. Two micro DC motors employing direct gears and two wheels with diameter of 2.2 cm actuate Colias with a maximum speed of 35 cm/s. However, in this design, we limited the speed of forward motion to 20 cm/s.

Motors are controlled individually using a pulse-width modulation (PWM) technique [38]. Each motor is driven separately by a H-bridge DC motor driver, and consumes power between 120 mW and 550 mW depending on the load. Colias uses three IR proximity sensors to avoid collisions with obstacles and other robots within less than 10 mm.

In Colias, the lower board is responsible for managing the power consumption as well as recharging process. Power consumption of the robot under normal conditions (in a basic arena with only walls) and short-range communication (low-power IR emitters) is about 2000 mW. However, it can be reduced to approximately 750 mW when IR emitters are turned on occasionally. A 3.7 V, 600 mAh (extendible up to 1200 mAh) lithium-polymer battery is used as the main power source, which gives an autonomy of approximately 2 hours for the robot.

B. Bio-inspired Vision Module

The vision module consists of two main parts: i) a compact camera module and ii) the main microprocessor. The schematic architecture of the vision module is illustrated in Fig.2. The power consumption of each part in the system are listed in TABLE.I.

1) Camera: A low voltage CMOS image sensor OV7670 module is utilised for it is a low-cost camera with a compact package size of 8×4 mm³ with 24-pin flexible flat fable (FFC) connector. The power supply is 3.3 V with active power consumption of 60 mW. The camera is capable of operating up to 30 frames per seconds (fps) in VGA mode with output support for RGB565, RGB888 and YUV422. The horizontal viewing angle is approximately 70°. All these features make the camera suitable for a miniature size mobile robot. As a trade-off for image quality and memory space, we choose a resolution of 72×99 pixel at 30 fps, with output format of 8-bit YUV422.

The digital interfaces used for configuration and data transmission include three groups which are a serial camera control bus (SCCB) with two wires for camera configuration, four clock/timing signals and an 8-bit parallel port for image data transferring.

2) Embedded Microprocessor: An ARM® Cortex™-M4F core micro-controller is deployed as the main processor for serving the image processing and monitoring all the modules including the camera, Colias platform and other sensors. The 32-bit Micro Control Unit (MCU) STM32F407 clocked at 168 MHz provides the necessary computational power to have a real-time image processing. The total SRAM capacity is 192 KByte.

The images captured by the camera are transmitted through the digital camera interface (DCMI) which is an embedded camera interface. It is connected to the camera module with CMOS sensors through an 8-bit parallel interface to receive image data. The camera interface sustains a data transfer rate up to 54 Mbyte/s at 54 MHz, paced by several synchronizing signals. Images received by DCMI are transmitted into SRAM through a direct memory access (DMA) channel. Fig.2 shows the proposed architecture of the hardware.

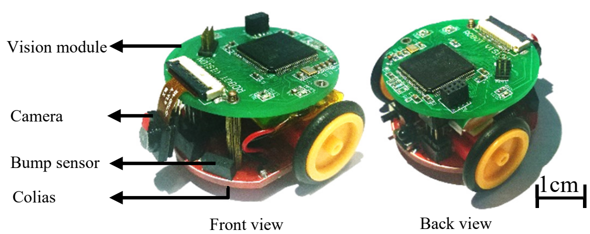

Fig. 2. Hardware architecture of the extension vision module.

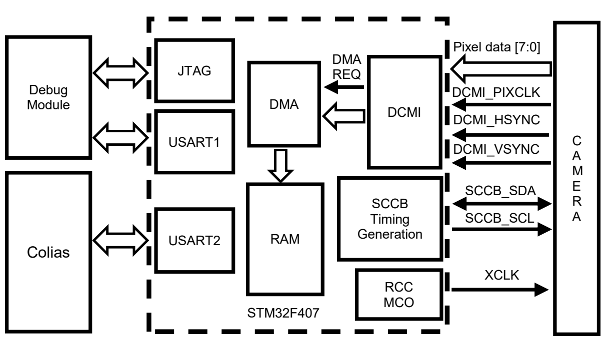

Fig. 3. The developed micro-robot with the vision module. The vision module (green) is placed on top of the robot platform Colias (red).

IV. PROPOSED COLLISION DETECTION METHOD

In this section, the proposed LGMD-based collision detection model, and the implementation of the model on the embedded micro-controller are described in detail.

A. LGMD Based Neural Model

The LGMD algorithm used in this work is based on the previous model proposed by Yue and Rind [19], as shown in Fig.4.

In order to reduce the computational complexity to fit the embedded processor, some simplification and approximation need to be applied in the algorithm, which will be described in the following sections.

The model is composed of five groups of cells, which are *P-cells* (photoreceptor), *I-cells* (inhibitory), *E-cells* (excitatory),

TABLE I
THE POWER CONSUMPTION CHARACTERISTICS

Description	typical	max	unit
Processor standby	18.5		
Processor active	111	148	
Camera standby	20		mW
Camera active	166.5	185	
Robot platform processor and sensors	29.6	111	
DC Motor x2	74	222	

S-cells (summing) and *G-cells* (grouping) and also two individual cells, namely, the feed-forward inhibitory (FFI) and LGMD.

The first layer of the neuron is composed by the *P* cells, which are arranged in a matrix. They are formed by the change of luminance in adjacent frames captured by the camera. In [19], the *P* layer was defined by:

$$\begin{aligned} P_f(x,y) &= L_f(x,y) - L_{f-1}(x,y) \\ &\quad + \sum_i^{n_p} p_i P_{f-i}(x,y) \qquad (1) \\ p_i &= (1+e^{\mu i})^{-1} \qquad (2) \end{aligned}$$

where n_p defines the maximum number of frames (or time steps) the persistence of the luminance change can last, the persistence coefficient $p_i \in (0,1)$. $P_f(x,y)$ is the change of luminance of each pixel at frame *f*, $L_f(x,y)$ and $L_{f-1}(x,y)$ are the luminance in current and the previous frames.

In this paper, *P* layer is defined simply by:

$$P_f(x,y) = L_f(x,y) - L_{f-1}(x,y) \qquad (3)$$

Comparing to the original algorithm (1), the visual persistence part which occupies a lot of computation power is removed.

The output of *P* cells serve as the inputs to two separate cell types in the next layer. One is the excitatory cells, through which excitation is passed directly to the retinotopic counterpart of the cell in the third layer.

$$E_f(x,y) = P_f(x,y) \qquad (4)$$

The second type of the cells are lateral inhibition cells which pass inhibition after one image frame delay to their retinotopical counterpart's neighbouring cells in the *E* layer. This layer is treated as a convolution operation:

$$[I]_f = [P]_f \otimes [w]_I \qquad (5)$$

where $\otimes$ stands for the convolution operation. It could also be written as:

$$I_f(x,y) = \sum_i \sum_j P_{f-1}(x+i)(y+j) w_I(i,j) \qquad (6)$$

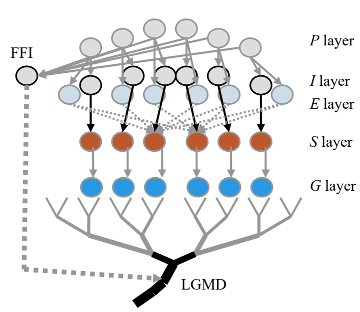

Fig. 4. A schematic of the LGMD based neural network for collision detection. The input of the *P* cells is the luminance change. Lateral inhibition is indicated with dotted lines and has one frame delay. Excitation is indicated with black lines which has no delay. The FFI cell has one frame delay.

where $[w]_I$ is the convolution mask that representing the local inhibiting weight spreading from the centre cell of *P* layer to neighbouring cells in *S* layer, given by:

$$[w]_I = \begin{bmatrix} 0.125 & 0.25 & 0.125 \\ 0.25 & 0 & 0.25 \\ 0.125 & 0.25 & 0.125 \end{bmatrix} \qquad (7)$$

The excitation of *E* cells and the inhibition of *I* cells are combined in the *S* layer by a subtraction. Usually the subtraction is given by:

$$s_f(x,y) = E_f(x,y) - I_f(x,y) * W_I \qquad (8)$$

where W_I is the inhibiting coefficient. However, the subtraction should be taken care of when the excitation and inhibition value of a pixel have opposite signs. In this case, (8) could lead to a false positive pixel in the *S* layer instead of the expected inhibition. We added a judgement to prevent this effect:

$$s_f(x,y) = E_f(x,y) - I_f(x,y) * W_I \qquad (9)$$

$$S_f(x,y) = \begin{cases} 0 & \textit{if} E_f(x,y) * I_f(x,y) \le 0 \\ s_f(x,y) & \textit{otherwise} \end{cases} \qquad (10)$$

The *G* layer is introduced to the model in order to reduce noise from the background. When reaches the *G* layer from *S* layer, the expanded edges which are represented by clustered excitations are enhanced to extract colliding objects against complex backgrounds. This mechanism is implemented with a passing coefficient for each cell, which is defined by a convolution operation in the *S* layer. The passing coefficient Ce is determined by the surrounding pixels, given by:

$$[Ce]_f = [S]_f \otimes [w]_e \qquad (11)$$

where w_e represents the influence of its neighbours and this operation can be simplified as a convolution mask:

$$[w_e] = \frac{1}{9} \begin{bmatrix} 1 & 1 & 1 \\ 1 & 1 & 1 \\ 1 & 1 & 1 \end{bmatrix} \qquad (12)$$

The excitation correspond to each cell $G_f(x,y)$ then becomes:

$$G_f(x,y) = S_f(x,y) Ce_f(x,y) \omega^{-1} \qquad (13)$$

where ω is a scale and computed at every frame:

$$\omega = 0.01 + \max \left| [Ce]_f \cdot C_w^{-1} \right| \qquad (14)$$

in which C_w is a constant, and $\max |[Ce]_f|$ is the largest absolute value of C_e.

The *G* layer is followed by a threshold set to filter decayed excitations:

$$\tilde{G}_f(x,y) = \begin{cases} G_f(x,y) & \textit{if } G_f(x,y) C_{de} \ge T_{de} \\ 0 & \textit{otherwise} \end{cases} \qquad (15)$$

where C_{de} is the decay coefficient which $C_{de} \in (0,1)$, T_{de} is the decay threshold. This grouping process can not only enhance the edges, but also filter out background detail caused excitations. The membrane potential of the LGMD cell K_f at frame f is calculated:

$$K_f = \sum_x \sum_y \left| \tilde{G}_f(x, y) \right| \tag{16}$$

Then K_f is transformed through a normalizer. In previous LGMD models, the normaliser function is given as a sigmoid function of:

$$\kappa_f = (1 + e^{-K_f n_{cell}^{-1}})^{-1} \tag{17}$$

where n_{cell} is the counting of pixels in the frame.

However, since K_f values are always positive, only the right part of the function (17) was used in the model, and the meaningless small inputs are not inhibited. Considering of inhibit small inputs, a similar normalising function is adopted instead, given by:

$$\kappa_f = \frac{\tanh(\sqrt{K_f} - n_{cell} C_1)}{n_{cell} C_2} \tag{18}$$

where C_1 and C_2 are constants to shape the normalizing function, limiting the excitation κ_f varies within $[0, 1]$. This function reduces noise for small K_f inputs and have adjustable sensitivity. A comparison test between these two normalizing functions are shown in Fig.5. The test is based on videos taken by real robots in the experiment setups described in Section V.

If the normalised value κ_f exceeds the threshold, then a spike is produced

$$S_f^{spike} = \begin{cases} 1 & \textit{if } \kappa_f \geq T_s \\ 0 & \textit{otherwise} \end{cases} \tag{19}$$

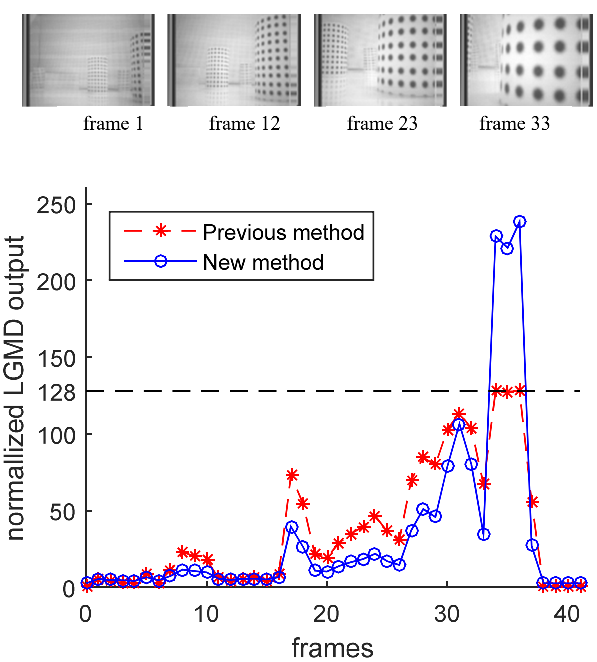

Fig. 5. Comparison of two types of normalizing functions in the model. The testing video is a robot captured video in a complex environment. The proposed method showed a better separation of small signals and big signals. The previous method reached the full scale at frame 33-35.

An impending collision is confirmed after n_{sp} (in our tests, four) successive spikes generated

$$C_f^{LGMD} = \begin{cases} 1 & \textit{if } \sum_{f-n_{ts}}^{f} S_f^{spike} \geq n_{sp} \\ 0 & \textit{otherwise} \end{cases} . \tag{20}$$

Normally, the robot's obstacle avoidance behaviour is depended on the value of C_f^{LGMD}. However, it is not surprised during turning, the neuron network may produce spikes and even false collision alerts because of the sudden change in the visual scene. The feed forward inhibition and lateral inhibition work together to cope with such whole field movement.

The FFI cell is proportional to the summation of excitations in all cells with one frame delay.

$$F_f = \sum_x \sum_y (|P_{f-1}(x, y)|) n_{cell}^{-1} \tag{21}$$

A spike of FFI cell is produced as soon as F_f exceeds its threshold T_{FFI}.

$$C_f^{FFI} = \begin{cases} 1 & \textit{if } F_f \geq T_{FFI} \\ 0 & \textit{otherwise} \end{cases} \tag{22}$$

In our case, the FFI output as well as the LGMD output both contribute to the decision of motion made by the robot.

The initial values for each parameters are listed in TABLE.II.

B. Realization of LGMD Model on Embedded System

As described in the previous sections, the LGMD-based collision detection system only involves the low level image processing such as excitation transferring and neighbouring operation. Traditional image processing methods containing computationally expensive methods are not used, such as object recognition or scene analysis. As a result, the model is ideal to be used by the embedded platforms. However, it is still not an easy task to optimise the memory consumption and timing for real-time application.

TABLE II
INITIAL PARAMETERS OF LGMD BASED NETWORK

Name	Value	Description	Name	Value	Description
W_I	0.4	Inhibition coefficient of inhibition layer	C_w	4	Grouping decaying strength
C_{de}	0.5	Grouping layer threshould	T_{FFI}	80	Threshould of FFI output
T_{de}	15	Grouping coefficient	T_s	100	Spiking threshould for LGMD
n_{cell}	7128	Number of cells	n_{sp}	4	LGMD spike number count
C_1	10	Constant for nomalization	C_2	11	Constant for nomalizatio

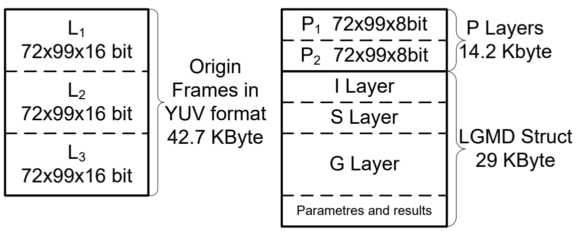

Fig. 6. Memory allocation of the micro-controller for images and LGMD structures.

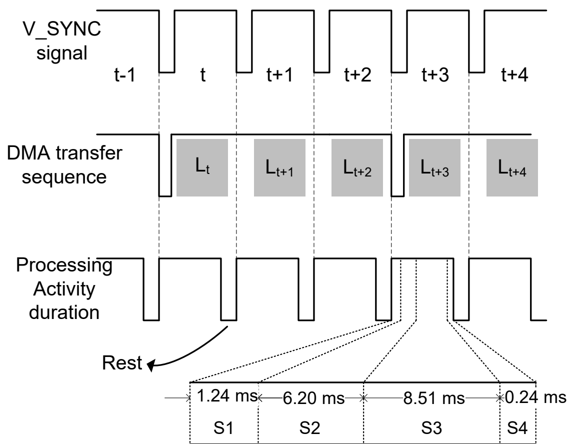

Fig. 7. Timing diagram for LGMD model processing. DMA transfer starts every 3 V_SYNC signals from the camera and last for 3 whole frames to capture the full image. LGMD model processing is triggered by each V_SYNC signal.

1) *Memory Management:* Fig.6 shows the memory allocation of LGMD model and related image buffers. For each individual LGMD process, at least two differential images (*P* layer) are required, and each *P* layer is calculated by two continuous frames. Accordingly, three image buffers are allocated to store the original frames from the camera. In this case, transferring of images and LGMD model processing can be performed simultaneously. In an individual LGMD structure, the *I* layer and the *S* layer are formed by 8-bit cells, the *G* layer is formed by 16-bit cells. In addition, the system is able to support multiple LGMD models with different region of interests (ROIs) due to the sharing of the public *P* layers. The total usage of SRAM is up to 100 KB in this application.

2) *Timing and Triggering Setup:* The processing inside the micro-controller is paced by a specific external pulse generated by the camera called Vertical Synchronization(VSYNC), which is active low when a new frame begins. The DMA sequence which used for automatically import images from camera to the SRAM is triggered every three VSYNC pulses. Thus three consecutive images are imported continuously with a single triggering. Meanwhile, the LGMD processing is triggered in each frame. In this way, the LGMD processing will always get fresh frames at any time instead of waiting for them.

As a real-time system, the total LGMD processing time must be limited within 33 ms, which is the duration of a single frame. To achieve this goal, all the calculations are divided into four states: S1 to S4. S1 mainly calculates the *P* layer based on the raw frame data. Then in S2, we can get *S* layer following by the *I* layer. After that, in S3, the grouping method is applied on the *S* layer. The LGMD cell and the following motion commands are worked out in S4. The FFI cell is computed in S2 separately by *P* layer of the former frame. In our tests, the LGMD processing took around 16 ms, guaranteed the possibility of real-time processing, as revealed in Fig.7. Fig.8 illustrates how the image transferring and processing are managed at different frames and the layer dependence.

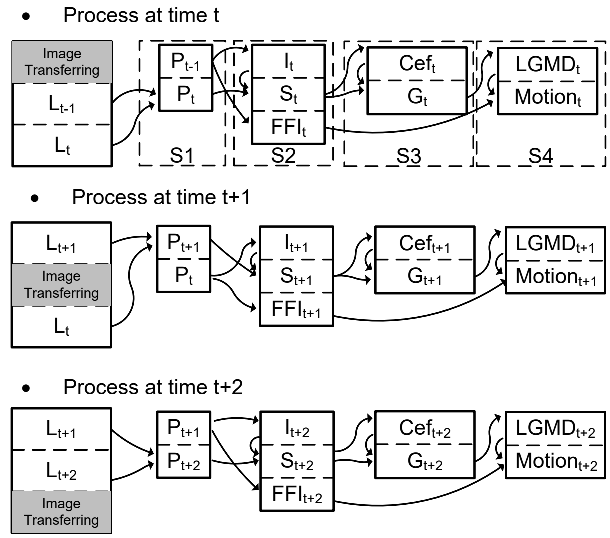

Fig. 8. Processing sequences for different frames. The state of the processing are shown as dashed boxes. Arrows represents the dependency of each data blocks.

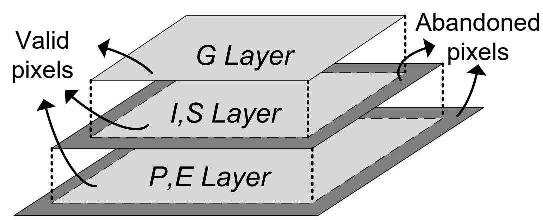

Fig. 9. The illustration of dealing the image boundaries in different layers.

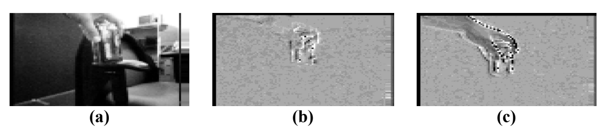

Fig. 10. Different layers of LGMD processing in an off-line test. (a) shows the original image, which is a hand waving a bottle in front of the camera; (b) shows the output of *P* layer. The background detail is inhibited, whereas the hand with the bottle stands out; (c) shows the output of *G* layer.

3) *Image Boundary Issues:* There are two convolution operations for layers in the LGMD model, which are the computation of *I* layer and the grouping coefficient *Ce*. There is always an issue with convolutions at edge pixels due to the mismatch between the image and mask shapes. Normally

there are two approaches to deal with this problem: i) copy from adjacent valid pixels and ii) ignore the edge pixel. We choose to abandon the edge pixels for time optimisation. As a result, the size of I and S layers are limited at 70×97 pixels, 2 pixels less in both width and height than the P layer. The G layer is even smaller, given by 68×95 pixels. Fig.9 shows the structure of the layer size. The example of different layers in the LGMD process are illustrated in Fig.10.

V. Experiments and Results

Several experiments are performed to test the sensitivity and robustness of the system. The first phase is LGMD processing test which mainly focused on the performance of the algorithm. The second phase is to investigate of the system that combined with motion controlling methods.

A. Experiments with Video Simulated Moving Object

Experiments with simulated moving object are the first phase of the experiments with a visual stimuli repeated for several times.

The video sequence used in the following experiments were generated by MATLAB in advance. The simulated object is a rectangle, which changes its width and height periodically, given as:

$$\begin{cases} Width_t = \lambda_W(-\cos(\pi f \cdot t)) + Width_0 \\ Height_t = \lambda_H(-\cos(\pi f \cdot t)) + Height_0 \end{cases} \tag{23}$$

where f stands for a constant that is related to the frame rate. Frame rates of 60 fps is used in the experiments. Value λ_W and λ_H are the scale factors for the object's dimensions. Details of the video sequence are described in Fig.11 (a). The video sequences were displayed on a LCD screen with a resolution of 1024×768 pixels (38 cm×31 cm). The experiments are accomplished in real time. The motion controlling function is disabled in this phase of experiments.

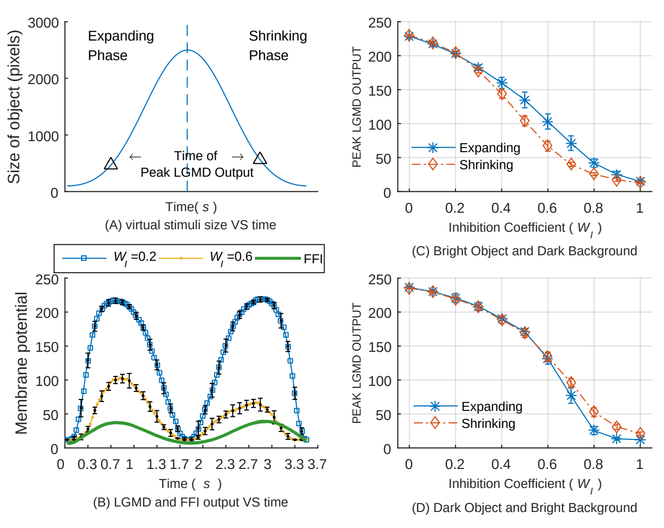

Fig. 11. Results of experiments with simulated moving object. (a) Size of the virtual moving object changes against time. The two triangles shows the time when peak LGMD outputs were generated. (b) Typical LGMD and FFI outputs sequence in the experiments with specified parameters. (c) and (d) The peak LGMD outputs in each experiments with different Inhibition coefficient. The blue solid results are peaks when object expanding, the brown dashed marks the peak values when objects shrinking. In (c), the moving object was bright (brightness 80%) in front of a dark background (brightness 10%). However in (d), the object is dark (brightness 20%) and the background is bright (brightness 70%).

Video sequences were generated with different background and object contrasts. In every sequence, both background and the simulated object have a certain brightness ranging from 0% (totally dark) to 100% (full bright).

We investigated the relationship between the LGMD output and the inhibiting coefficient W_I in the LGMD model. The W_I ranged from 0 to 1. The results depicted in Fig.11 reveals that the LGMD output is strongly related to W_I value. In addition, the direction selective ability of the model can be observed in the results. The peak output of LGMD model in the expanding phase is greater than which in the receding phase when the background is brighter than the object, and it is smaller when the background is darker than the object.

B. Preliminary Functioning Tests

In order to confirm whether the embedded LGMD model is able to deal with collision situation in real world applications, several experiments for basic and typical collision situations are designed.

Three types of collision situations are considered which are: i) objects moving towards the robot on a collision trajectory, ii) objects approaching the robot with a slight angle off the collision course, called the *"near miss"* objects and iii) robot moving towards a wall.

1) Approaching Object: One of the challenges that a real locust has to deal with is the approaching predator in front. Hence, the LGMD neuron network of our robot should demonstrate similar characteristics as that of a real locust does when facing similar challenges.

A rolling tennis ball towards the robot acted as the predator in the tests. The tennis ball (diameter 66 mm) has fury green surface with white strips, which provide identifiable texture details needed for the robot. The rolling speed of the tennis ball is controlled. It rolls down along a tilted wooden plank with a adjustable inclination angle of θ degree, as illustrated in Fig.12. A guide track, which sits diagonally to the tilted plank, allows the ball roll down along a certain trajectory starting from a rest status. Since the inclination θ is small, the speed of rolling ball is considered as constant determined by θ. The

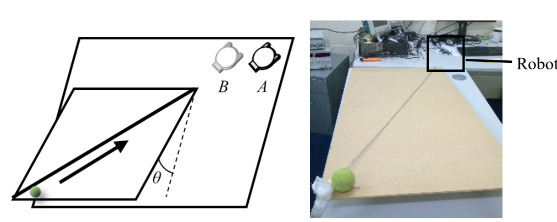

Fig. 12. Testing table for LGMD processing. In approaching object tests, the robot (A) is placed on the table surface, fixed in the trajectory of the tennis ball in the first experiment; and different distances away from the trajectory in the "near miss" object tests. (b) experiment setup. The vision module is at the upright corner of the photo, marked with a box.

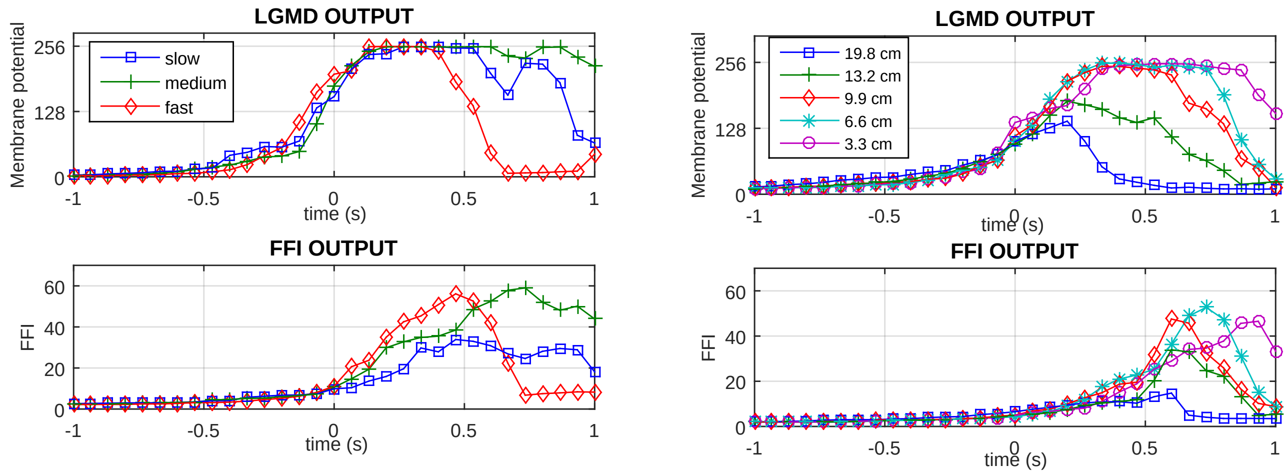

(a) (b)

Fig. 13. Average records for each set in experiment with approaching object and near miss object. Both LGMD and FFI outputs are shown. The x axis represents time in seconds, y axis is for neuron network output. Records are aligned at when the outputs exceed LGMD threshold, which are set time zero. (a) records of approaching object experiments with different speed; (b) records of passing object experiments with different offset from the robot.

robot is protected by a plastic frame in order to prevent it from being knocked down by the ball.

In each test, the robot is fixed on the table, facing the rolling ball and the outputs of both LGMD and FFI are recorded. Several set of experiments were carried out with different θ giving different terminal approaching speed respectively.

The results of these experiments are shown in Fig.13(a). We observed that the model has been functioning appropriately in every set of experiments - alerts have been triggered by the approaching ball at different speeds.

2) Near Miss Object: The next experiment is designed for testing the behaviour of the LGMD model when object brushes by. In this case, the generated hazardous level depends on how close the robot can be from the near miss object.

Based on the first testing environment, we adjust the placement of robot aside from the trajectory with adjustable offset S. As in the previous tests, the running trajectory and speed settings of the tennis ball are kept the same.

Experiments with five different offsets S are conducted one by one respectively. For each offsets S, 15 repeated experiments have been done to capture the outputs of the LGMD and the FFI. Results are shown in Fig.13(b).

From the records we can find out that the LGMD output in each test increases as the ball approaches the robot, indicating the increasing risk of collision. However, soon after the ball moves out of sight, the LGMD output drops immediately. The FFI output also accumulates when the outputs of LGMD is increasing.

3) Distance to Collision: The performance of the obstacle avoidance behaviour varied under different moving speeds. It is important to estimate the distance between the robot and the obstacle when the LGMD model generates turning command while approaches a certain obstacle. This distance is often called the distance to collision.

To simplify the testing conditions, the robot is allowed to run towards a textured wall. Robot starts running 50 cm away from the wall until the turning commands triggered. Experiments are with nine different speeds ranging from 1.5 cm/s to 17 cm/s. The results are shown in Fig.14.

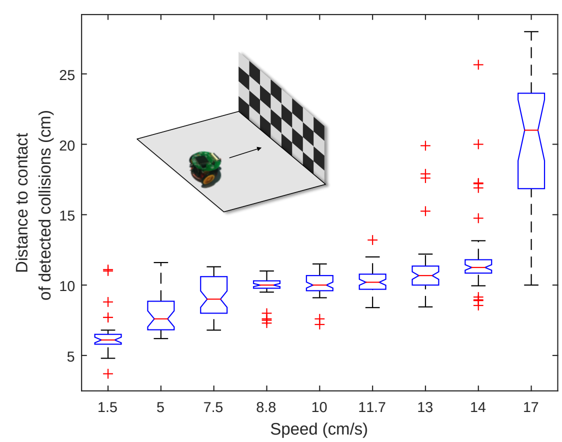

Fig. 14. Results in diagram of the tests of distance to collision vs speed of the robot. For each group of data, the central mark is the median, blue square is formed by the first and third quartiles. Outliers are represented by red pluses.

The results show that the distances to collision increase as the robot moves faster. When speed is between 5 cm/s and 14 cm/s, the robot performed consistently. When the robot moves at a high speed (e.g., 17 cm/s), more fake alarms are generated, due to the shaky movement and blurred images.

C. Real World Tests

In the previous phase of the experiments, we showed the ability of embedded LGMD model that can detect looming stimuli, while the obstacles and scenes remained unchanged in these tests.

However, in any real world applications, the vision system, working with other components of the robot such as motor control system, should cope with complex scenarios without compromise in collision detection. Thus we designed several experiments to test the robustness of the integrated vision system. Before doing these experiments, we introduced some motor commands to setup basic robot behaviours.

1) Motor Commands Description: In the real world tests, LGMD algorithm works together with motor commands, which are described below.

There are three types of motor control commands which are 'F' for going forward, 'L' or 'R' for turn left or right and 'S' for stop. The decision is triggered by both LGMD and FFI outputs.

As shown in the Table.III, if the output of LGMD and FFI both stay 0 – means the environment is safe for robot to go forward, the command 'F' will be given to the motor control unit. When a collision is going to happen, the LGMD cell is triggered while the FFI remains silent, the 'L' or 'R' will be given to the motor control unit allowing the robot turns immediately to avoid collision. During turning phase, FFI would be triggered due to whole-frame movement, a command 'S' is sent out to stop the robot immediately once the current executing command finished.

The turning speed ω is a constant so the turning angel θ_{turn} can be determined simply by the action duration, given by

$$\theta_{turn} = T_{turn} * \omega \tag{24}$$

$$T_{turn} = (6 + rand(4)) \cdot T_p \tag{25}$$

$$\omega \approx 2\pi \ rad/s \tag{26}$$

where T_p is the duration of a frame, which is around 33 ms, $rand(4)$ is a random number generator that generates random number ranging [0, 4]. Therefore, the time period of turning is around 200 ms to 400 ms and the turning angle is ranging from 70°to 140°.

It must be noted that, since LGMD cell cannot tell where the object exactly is, the turning direction have to be chosen randomly. To imitate a real animal behaviours and avoid swing from side to side, the robot is set to have a preference of turning right (80%) than turning left (20%).

TABLE III
CONTROL COMMANDS DEFINITION

Neuron Status C_f^{LGMD}	C_f^{FFI}	Decision	Command word
0	0	Go forward	'F'
1	0	Turn left or right	'L' or 'R'
X(any value)	1	Stop	'S'

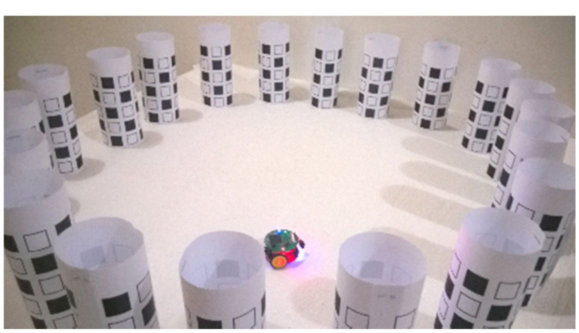

Fig. 15. The setup of the arena for the experiment surrounded by poles.

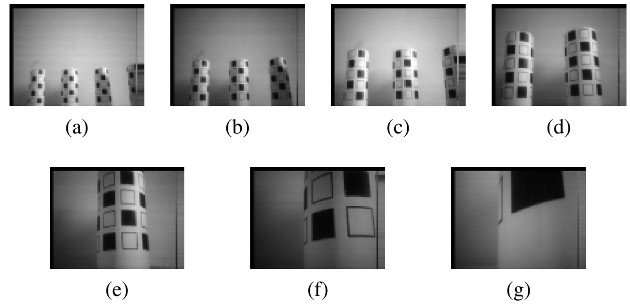

Fig. 16. Sample frames taken by the robot on the trajectory approaching the paper poles during the experiment. Distances from the robot are 60 cm (a), 50 cm (b), 40 cm (c), 30 cm (d), 20 cm (e), 10 cm (f) and 5 cm (g) respectively.

2) Experiments of Robot Surrounded by Textured Poles: In the first real world test, the robot is challenged in an arena surrounded by several paper poles. The paper poles are curled by A4 sized paper, which textured with black and white squares, as shown in Fig.15. The surrounded area has a diameter of approximately 70 cm.

As mentioned earlier, the LGMD based collision detection system can deal with complex situations. The background used in the experiments are kept as it is without control. The robot moved at the speed of about 10 cm/s in the arena and it turns when imminent collision is detected.

The experiment lasted for 5 minutes. Sample results are shown in Fig.17, which shows series of the LGMD and FFI outputs during the test. Four imminent collisions were detected during the experiment at about 10s, 17s, 23s and 30s respectively. There are 4 peaks as shown in the Fig.17, indicating 4 collisions detected and 4 turns executed during this period of time. Sample images taken from the robot's camera in the test are shown in Fig.16.

3) Trapped Robot in "Paper Forest": We would like to investigate the collision avoiding performance in a more challenging environment with abundant of objects. Therefore, we built a new testing arena which is called the "paper forest", as shown in Fig.18.

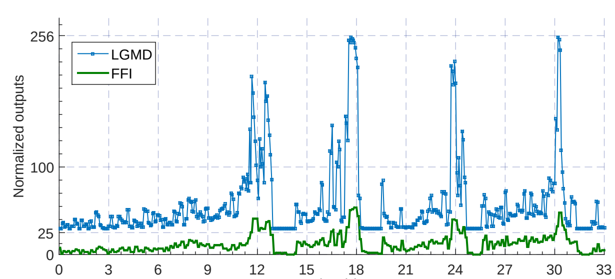

Fig. 17. Part of the normalised outputs of both LGMD and FFI during the experiment. The x axis represents the time in seconds and y axis is for the normalised outputs within [0, 1]. The upper blue trace shows the LGMD output; the FFI output is in black. During the time period, four successful turning was executed at around 10 s, 17 s, 23 s and 30 s.

The "paper forest" is a square arena with size of 95 cm by 115 cm, surrounded by walls of 40 cm height. The walls are decorated by textured papers. Up to 30 cylinder shaped obstacles with 4 cm diameter and 8 cm height are placed randomly inside the arena. These cylinders are made of polystyrene, weighting 7 grams each. They are not glued onto the floor, which makes them be easily pushed away by the robot if collision detection fails.

The robot is allowed to run autonomously inside the area. The embedded LGMD model is expected to detect the upcoming collisions and trigger the avoidance action as described above.

Two additional IR bump sensors provided by the Colias are enabled in the experiments. Both IR sensors are placed at the front part of the robot, facing 30° to the left and right with limited detection range of 10±2 mm. They are set to detect whether a head-on collision happens, by a blinking LED.

As a supplemental detecting method, the IR bumpers are not expected to be triggered frequently, as they were configured with short range (10 mm). Since the turning action(duration and speed) is different from which triggered by the LGMD model, it is easy to tell whether a collision detection is successful from recorded videos of experiments.

Several experiments are performed with different speeds and obstacle densities. Each experiment lasted for 10 minutes. The tested speeds range from 8.5 cm/s to 20.3 cm/s. The density of obstacles are considered as "sparse" if there were 7 obstacles inside the arena, "medium" if 18 obstacles inside and "dense" if 29 obstacles.

Inside the arena, the robot turns to left or right if an obstacle or wall on a collision course at a certain distance is detected. The IR bump sensors may be triggered if an obstacle is hit by the robot, which is treated a failure. In some cases, the obstacle is bumped by the wheel or the rear of the robot due to the limited field of view, which is not counted as a failure.

The trajectory of the robot and the position of obstacles during the tests are tracked and analysed by a real time tracking system [39] which has been developed for multiple

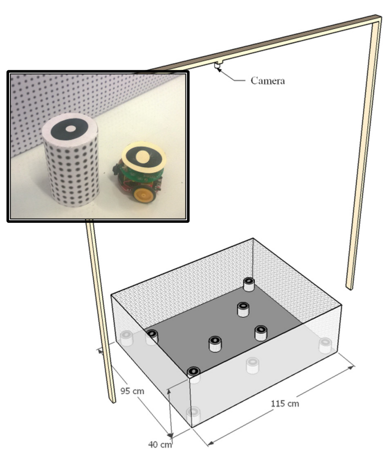

Fig. 18. The test arena and an image showing the wall, the obstacle and the robot.

robot localisation with sub-pixel precision. The ring patterns are placed on top of the robot and all the obstacles. The videos used for tracking are recorded by a Panasonic HD camera with resolution of 1280×720 at 60 fps. The camera is mounted above the experimental arena. In the experiments, the system tracks all of the objects simultaneously with accuracy of about 3 mm.

The robot trajectories are overlaid, as shown in Fig.19, and position distributions in each experiments are shown in Fig.20(a). Results proved that the robot has the ability to achieve continuous movements in different circumstances. The average success rate is above 95%, as given in Fig.20(b). The distribution of number of detections versus the distances to the obstacle at the time of turning action roughly correspond to normal distribution, as illustrated in Fig.20(c). These results suggested that the robot with embedded collision avoidance system can deal with dynamic and complex environments.

4) Dynamic Experiments with Two Robot: The ability of tolerating dynamic objects is proved by a series of experiments with two robots. In the experiments, two robots with the same configuration are initially placed 60 cm away facing to each other. The experiment setup and results are illustrated in Fig.21. The results prove that the robots are able to detect moving obstacles soon enough and trigger reasonable avoiding movements.

VI. FURTHER DISCUSSIONS

In this work, we presented an embedded vision module with LGMD based collision detection fitted on a micro-robot. The system demonstrated its reliability for collision detection and avoidance under challenges of dynamic scenarios. Comparing to previous robotics experiments featured with LGMD like collision detection such as Blanchard et al. [22] using Khepera mobile robot, Santer et al. [40] with Khepera mobile robot, Yue et al. [19] on Khepera II, A.C Silva et al. [33] with DRK8000 mobile robot and Badia et al. [31] on flying robots as well as on "Strider" [23], the most significant difference is that in this research the robot performed all the collision detection and avoidance autonomously within the on-board chips, no host PC is involved. With all the computation completed within the on-board system, the robot could be used in various situations for different purposes, such as swarm robotics research.

Being able to see and react to the complex visual world is one of the fundamental ability for many animal species which brings in numerous inspirations. In robotics, there have been different visual based navigation and guidance modules proposed [41]–[43]. Nowadays, as the image sensors and micro-controllers are becoming cheaper and more reliable, embedded vision modules are getting popular in intelligent device applications [28], [44]–[46] to enhance their navigation performance.

However, LGMD in locust is only one of hundreds of strong visual neurons in the lobula layer each may involve in specific visual tasks. There are other numerous neural networks in insects' brain engaged to extract the abundant visual cues simultaneously. The interaction of those neurons are still under

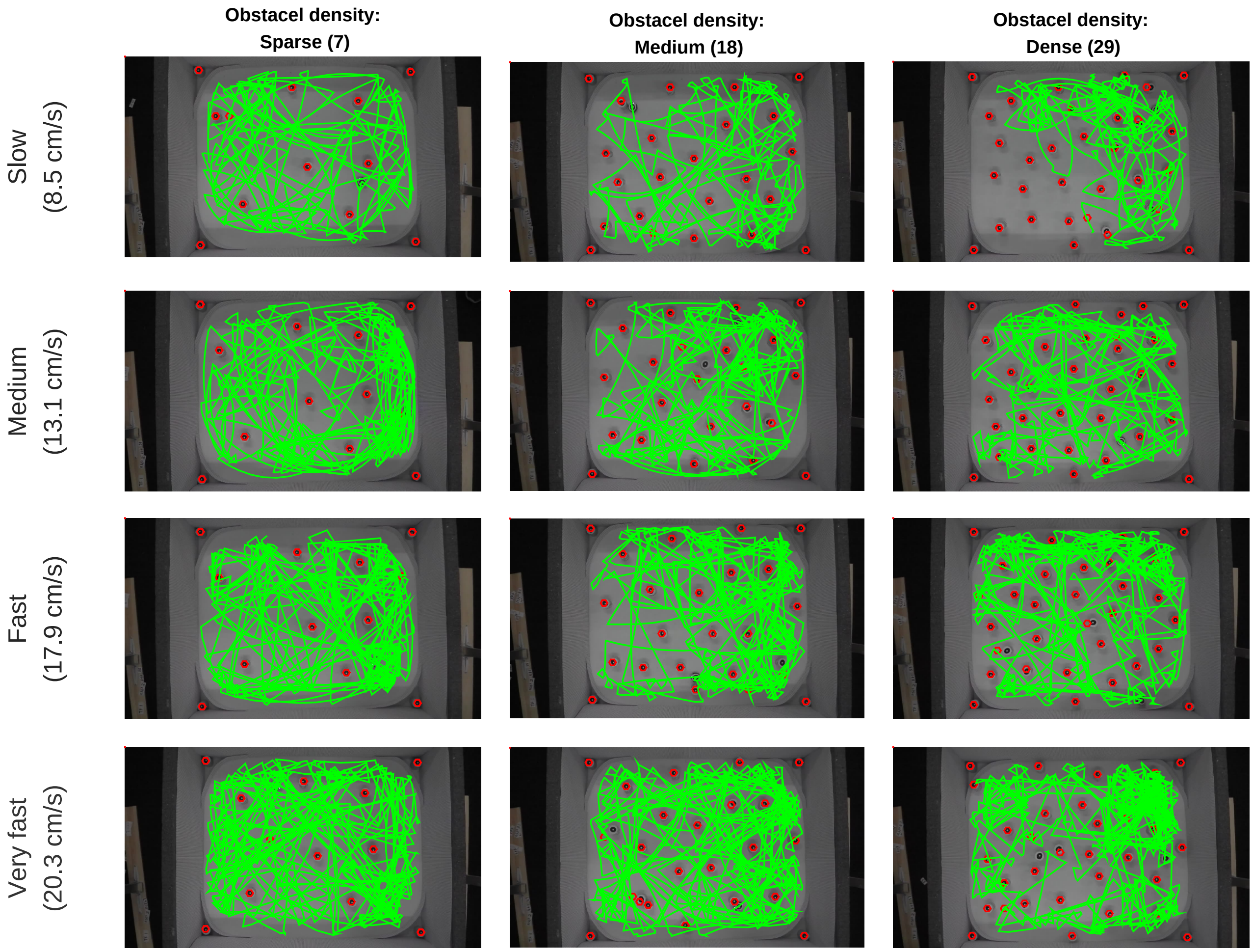

Fig. 19. The sample of trajectories of the robot in each experiment in the "forest". The green lines represent the trajectories of the robot. The initial place of the obstacles are shown as red circles.

investigation. Directional selective neurons [14], [17], [47], [48] which may be used to detect translating objects has been modelled and tested in [49] and [50], while [51] showed the combination of LGMD and DSNs. We hope that further implementations with several different neuron structures could lead robots respond to the dynamic world better.

The vision module proposed in this study can acquire and process images independently, it could fit to other robotic platforms or motion patterns easily with slight modification. For example, with the merging of reflex mechanism or central pattern generator(CPG), the module could be applied to crawling or walking robots [52], [53]. With the compacted size and limited power consumption, it is possible to integrate multiple vision modules into one robotic platform, for example, two modules to form a binocular robot vision system. High level algorithms such as sensor fusion could also be applied to improve the accuracy of collision detection.

VII. Conclusion

Reliable, low-cost, compact and low power consumption visual collision detection and avoidance system has been in the wishing list for mini or micro-robots for a long time yet in supply. In the above chapters, the presented realization of LGMD model on one compact board with ARM chip showed a step closer to satisfy these demands. As demonstrated via various experiments, the vision module is reliable in different environment settings for collision detection which allows the micro-robot to perform avoidance behaviours pertinently and timely. Since all the image acquisition and processing functionalities are completed on one compact board, the vision system can be easily integrated to the micro-robot and other similar mini-robotics systems as well. For future work, the vision module can be extended by integrating other bio-inspired neuron models for complex visual tasks, and for multiple robotics applications.

Acknowledgment

This work was supported by EU FP7 projects LIVCODE (295151), HAZCEPT (318907), HORIZON 2020 project STEP2DYNA (691154), National Natural Science Foundation of China (51335004) and 973 National Basic Research Program of China (2011CB013301).

References

[1] H. Everett, *Sensors for mobile robots: theory and application*. AK Peters, Ltd., 1995.

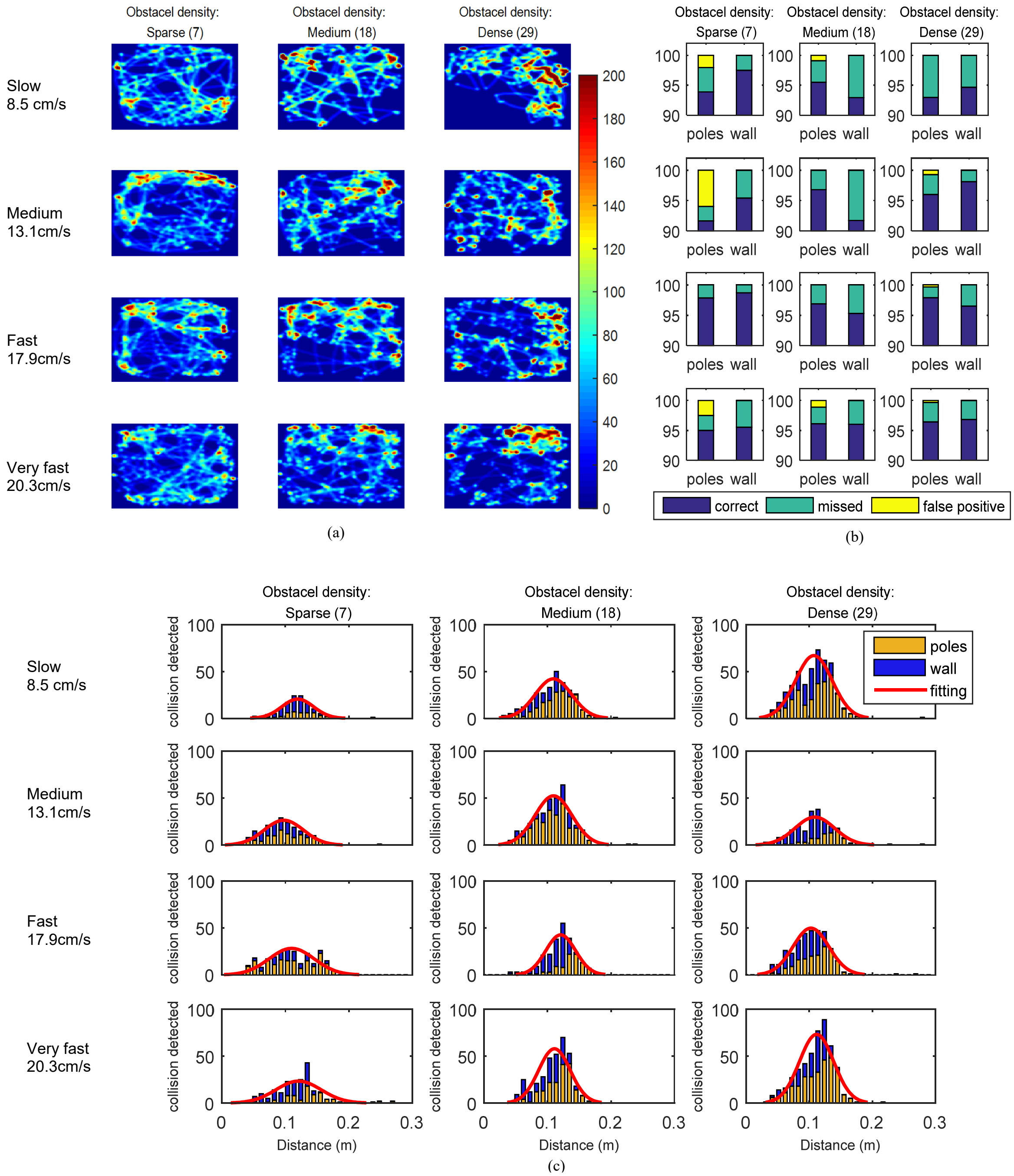

Fig. 20. Results of each experiment of robot in the “forest”. (a): the robot position distribution. (b): the success rate of each experiments. (c) The distribution of the distance to the obstacle when turning happens. Red curves showed the normal distribution fitting.

[2] G. Benet, F. Blanes, J. E. Simo, and P. Perez, “Using infrared sensors for distance measurement in mobile robots,” *Robotics and Autonomous Systems*, vol. 40, no. 4, pp. 255–266, 2002.

[3] F. Arvin, K. Samsudin, and A. R. Ramli, “Development of IR-based short-range communication techniques for swarm robot applications,” *Advances in Electrical and Computer Engineering*, vol. 10, no. 4, pp. 61–68, 2010.

[4] G. v. Wichert, “Can robots learn to see?” *Control Engineering Practice*, vol. 7, no. 6, pp. 783–795, 1999.

[5] R. Manduchi, A. Castano, A. Talukder, and L. Matthies, “Obstacle detection and terrain classification for autonomous off-road navigation,” *Autonomous Robots*, vol. 18, no. 1, pp. 81–102, 2005.

[6] S. Yue, R. D. Santer, Y. Yamawaki, and F. C. Rind, “Reactive direction control for a mobile robot: a locust-like control of escape direction emerges when a bilateral pair of model locust visual neurons are integrated,” *Autonomous Robots*, vol. 28, no. 2, pp. 151–167, 2010.

[7] H. Buxton, “Learning and understanding dynamic scene activity: a review,” *Image and Vision Computing*, vol. 21, no. 1, pp. 125–136, 2003.

[8] F. C. Rind and P. J. Simmons, “Seeing what is coming: building collision-sensitive neurones,” *Trends in Neurosciences*, vol. 22, no. 5, pp. 215–220, 1999.

[9] R. D. Santer, P. J. Simmons, and F. C. Rind, “Gliding behaviour elicited by lateral looming stimuli in flying locusts,” *J Comp Physiol A Neuroethol Sens Neural Behav Physiol*, vol. 191, no. 1, pp. 61–73, 2005.

[10] M. O’shea, C. Rowell, and J. Williams, “The anatomy of a locust visual interneurone; the descending contralateral movement detector,” *Journal of Experimental Biology*, vol. 60, no. 1, pp. 1–12, 1974.

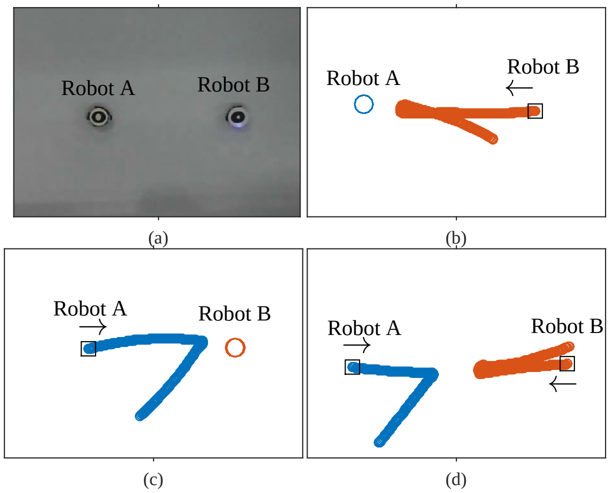

Fig. 21. Experiment setup and trajectories with two moving robots, namely A (left) and B (right). (a) The experiment setup. (b) Robot A is stationary, while robot B moves towards A. (c) Robot A moves towards the stationary B. (d) both A and B move towards each other. The initial places of moving robots are marked with a square. Their directions are shown with arrows.

[11] P. S. Bhagavatula, C. Claudianos, M. R. Ibbotson, and M. V. Srinivasan, "Behavioral lateralization and optimal route choice in flying budgerigars," *PLoS Comput Biol*, vol. 10, no. 3, p. e1003473, 2014.

[12] A. C. Paulk, J. A. Stacey, T. W. Pearson, G. J. Taylor, R. J. Moore, M. V. Srinivasan, and B. van Swinderen, "Selective attention in the honeybee optic lobes precedes behavioral choices," *Proceedings of the National Academy of Sciences of the United States of America*, vol. 111, no. 13, pp. 5006–11, 2014.

[13] S.-E. Yu and D. Kim, "Burrow-centric distance-estimation methods inspired by surveillance behavior of fiddler crabs," *Adaptive Behavior*, vol. 20, pp. 273–286, 2012.

[14] F. C. Rind, "A directionally selective motion-detecting neurone in the brain of the locust: physiological and morphological characterization," *Journal of Experimental Biology*, vol. 149, no. 1, pp. 1–19, 1990.

[15] F. C. Rind and P. J. Simmons, "Orthopteran dcmd neuron: a reevaluation of responses to moving objects. i. selective responses to approaching objects," *Journal of Neurophysiology*, vol. 68, no. 5, pp. 1654–66, 1992.

[16] S. Judge and F. Rind, "The locust dcmd, a movement-detecting neurone tightly tuned to collision trajectories," *Journal of Experimental Biology*, vol. 200, no. Pt 16, pp. 2209–16, 1997.

[17] F. C. Rind, "Identification of directionally selective motion-detecting neurones in the locust lobula and their synaptic connections with an identified descending neurone," *Journal of Experimental Biology*, vol. 149, no. 1, pp. 21–43, 1990.

[18] M. Blanchard, F. C. Rind, and P. F. M. J. Verschure, "Collision avoidance using a model of the locust lgmd neuron," *Robotics and Autonomous Systems*, vol. 30, no. 1-2, pp. 17–38, 2000.

[19] S. Yue and F. C. Rind, "Collision detection in complex dynamic scenes using an lgmd-based visual neural network with feature enhancement," *IEEE Transactions on Neural Networks*, vol. 17, no. 3, pp. 705–716, 2006.

[20] ——, "Near range path navigation using lgmd visual neural networks," in *2nd IEEE International Conference on Computer Science and Information Technology*. IEEE, 2009, Conference Proceedings, pp. 105–109.

[21] F. C. Rind and D. I. Bramwell, "Neural network based on the input organization of an identified neuron signaling impending collision," *Journal of neurophysiology*, vol. 75, no. 3, pp. 967–85, 1996.

[22] M. Blanchard, P. F. Verschure, and F. C. Rind, "Using a mobile robot to study locust collision avoidance responses," *International Journal of Neural Systems*, vol. 9, no. 05, pp. 405–410, 1999.

[23] S. B. i Badia, U. Bernardet, and P. F. Verschure, "Non-linear neuronal responses as an emergent property of afferent networks: a case study of the locust lobula giant movement detector," *PLoS computational biology*, vol. 6, no. 3, p. e1000701, 2010.

[24] F. Arvin, A. E. Turgut, F. Bazyari, K. B. Arikan, N. Bellotto, and S. Yue, "Cue-based aggregation with a mobile robot swarm: a novel fuzzy-based method," *Adaptive Behavior*, vol. 22, no. 3, pp. 189–206, 2014.

[25] F. Arvin, J. Murray, C. Zhang, and S. Yue, "Colias: An autonomous micro robot for swarm robotic applications," *International Journal of Advanced Robotic Systems*, vol. 11, p. 1, 2014.

[26] M. V. Srinivasan, R. J. Moore, S. Thurrowgood, D. Soccol, D. Bland, and M. Knight, *Vision and Navigation in Insects, and Applications to Aircraft Guidance*. MIT Press, 2014.

[27] M. V. Srinivasan, R. J. Moore, S. Thurrowgood, D. Soccol, and D. Bland, *From biology to engineering: insect vision and applications to robotics*. Springer, 2012.

[28] S. Saha, A. Natraj, and S. Waharte, "A real-time monocular vision-based frontal obstacle detection and avoidance for low cost uavs in gps denied environment," in *IEEE International Conference on Aerospace Electronics and Remote Sensing Technology*. IEEE, 2014, Conference Proceedings, pp. 189–195.

[29] F. A. Yaghmaie, A. Mobarhani, and H. D. Taghirad, "A new method for mobile robot navigation in dynamic environment: Escaping algorithm," in *First RSI/ISM International Conference on Robotics and Mechatronics*, 2013, Conference Proceedings, pp. 212–217.

[30] Z. Zhang, S. Yue, and G. Zhang, "Fly visual system inspired artificial neural network for collision detection," *Neurocomputing*, vol. 153, pp. 221–234, 2015.

[31] S. B. i. Badia, P. Pyk, and P. F. M. J. Verschure, "A fly-locust based neuronal control system applied to an unmanned aerial vehicle: the invertebrate neuronal principles for course stabilization, altitude control and collision avoidance," *The International Journal of Robotics Research*, vol. 26, no. 7, pp. 759–772, 2007.

[32] N. Franceschini, F. Ruffier, J. Serres, and S. Viollet, *Optic flow based visual guidance: from flying insects to miniature aerial vehicles*. IN-TECH Open Access Publisher, 2009.

[33] A. C. Silva, J. Silva, and C. P. d. Santos, *A Modified LGMD Based Neural Network for Automatic Collision Detection*. Springer, 2014, vol. 283, pp. 217–233.

[34] H. Y. Meng, K. Appiah, S. G. Yue, A. Hunter, M. Hobden, N. Priestley, P. Hobden, and C. Pettit, "A modified model for the lobula giant movement detector and its fpga implementation," *Computer Vision and Image Understanding*, vol. 114, no. 11, pp. 1238–1247, 2010.

[35] R. R. Harrison, "A biologically inspired analog ic for visual collision detection," *Ieee Transactions on Circuits and Systems I-Regular Papers*, vol. 52, no. 11, pp. 2308–2318, 2005.

[36] H. Okuno and T. Yagi, "A visually guided collision warning system with a neuromorphic architecture," *Neural Networks*, vol. 21, no. 10, pp. 1431–1438, 2008.

[37] F. Arvin, A. E. Turgut, T. Krajn'ik, and S. Yue, "Investigation of cue-based aggregation in static and dynamic environments with a mobile robot swarm," *Adaptive Behavior*, p. 1059712316632851, 2016.

[38] F. Arvin and M. Bekravi, "Encoderless position estimation and error correction techniques for miniature mobile robots," *Turkish Journal of Electrical Engineering and Computer Sciences*, vol. 21, no. 6, pp. 1631–1645, 2013.

[39] T. Krajník, M. Nitsche, J. Faigl, P. Vaněk, M. Saska, L. Přeučil, T. Duckett, and M. Mejail, "A practical multirobot localization system," *Journal of Intelligent & Robotic Systems*, vol. 76, no. 3-4, pp. 539–562, 2014.

[40] R. D. Santer, R. Stafford, and F. C. Rind, "Retinally-generated saccadic suppression of a locust looming-detector neuron: investigations using a robot locust," *Journal of the Royal Society Interface*, vol. 1, no. 1, pp. 61–77, 2004.

[41] D. Ognibene and G. Baldassare, "Ecological active vision: Four bioinspired principles to integrate bottom-up and adaptive top-down attention tested with a simple camera-arm robot," *IEEE Transactions on Autonomous Mental Development*, vol. 7, no. 1, pp. 3–25, 2015.

[42] S. Ivaldi, N. Sao Mai, N. Lyubova, A. Droniou, V. Padois, D. Filliat, P. Y. Oudeyer, and O. Sigaud, "Object learning through active exploration," *IEEE Transactions on Autonomous Mental Development*, vol. 6, no. 1, pp. 56–72, 2014.

[43] S. Boucenna, S. Anzalone, E. Tilmont, D. Cohen, and M. Chetouani, "Learning of social signatures through imitation game between a robot and a human partner," *IEEE Transactions on Autonomous Mental Development*, vol. 6, no. 3, pp. 213–225, 2014.

[44] J. Park and Y. Kim, "Stereo vision based collision avoidance of quadrotor uav," in *12th International Conference on Control, Automation and Systems*. IEEE, 2012, Conference Proceedings, pp. 173–178.

[45] I. Lenz, M. Gemici, and A. Saxena, "Low-power parallel algorithms for single image based obstacle avoidance in aerial robots," in *IEEE/RSJ International Conference on Intelligent Robots and Systems*. IEEE, 2012, Conference Proceedings, pp. 772–779.

[46] J. Kim and Y. Do, "Moving obstacle avoidance of a mobile robot using a single camera," *Procedia Engineering*, vol. 41, pp. 911–916, 2012.
[47] A. Borst and J. Haag, "Neural networks in the cockpit of the fly," *Journal of Comparative Physiology A*, vol. 188, no. 6, pp. 419–437, 2002.
[48] S. F. Stasheff and R. H. Masland, "Functional inhibition in direction-selective retinal ganglion cells: spatiotemporal extent and intralaminar interactions," *Journal of Neurophysiology*, vol. 88, no. 2, pp. 1026–1039, 2002.
[49] S. Yue and F. C. Rind, "A synthetic vision system using directionally selective motion detectors to recognize collision," *Artificial Life*, vol. 13, no. 2, pp. 93–122, 2007.
[50] ——, "Postsynaptic organisations of directional selective visual neural networks for collision detection," *Neurocomputing*, vol. 103, pp. 50–62, 2013.
[51] ——, "Redundant neural vision systemsompeting for collision recognition roles," *IEEE Transactions on Autonomous Mental Development*, vol. 5, no. 2, pp. 173–186, 2013.
[52] G. Li, H. Zhang, J. Zhang, and H. P. Hildre, "An approach for adaptive limbless locomotion using a cpg-based reflex mechanism," *Journal of Bionic Engineering*, vol. 11, no. 3, pp. 389–399, 2014.
[53] C. Liu, Q. Chen, and G. Wang, "Adaptive walking control of quadruped robots based on central pattern generator (cpg) and reflex," *Journal of Control Theory and Applications*, vol. 11, no. 3, pp. 386–392, 2013.

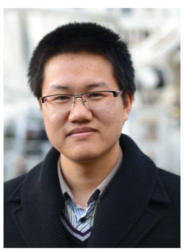

Cheng Hu received the BEng degree in College of Opt-electronics engineering from Chongqing University, Chongqing, China in 2013. He is currently pursuing the PhD degree in School of Computer Science, University of Lincoln, Lincoln, UK. His research interests include autonomous robots, sensors and signal processing. He was awarded a Marie Curie Fellowship to be involved in the FP7- EYE2E and LIVCODE projects during his Ph.D. study. He visited the Institute of Microelectronics at Tsinghua University in Beijing, China from March 2014 to August 2014 as a research assistant under the supervision of Professor Chun Zhang. He visited the Institute of Rehabilitation and Medical Robotics in Huazhong University of Science and Technology (HUST), Wuhan, China in 2014 under the supervision of Professor Caihua Xiong.

Farshad Arvin is a Research Associate at the School of Electrical and Electronic Engineering at The University of Manchester, UK. He holds a Ph.D. in Computer Science from University of Lincoln, UK. He was a research assistant at the Computational Intelligence Laboratory (CIL) at the University of Lincoln under the supervision of Professor Shigang Yue. He received his B.Sc. degree in Computer Engineering and M.Sc. degree in Computer Systems Engineering in 2004 and 2010, respectively. His research interests include autonomous robots, swarm robotics and signal processing. He was awarded a Marie Curie Fellowship to be involved in the FP7- EYE2E and LIVCODE projects during his Ph.D. study. He visited the Institute of Microelectronics at Tsinghua University in Beijing, China from September 2012 to August 2013 as a senior scholar under the supervision of Professor Zhihua Wang. He visited the Institute of Rehabilitation and Medical Robotics in Huazhong University of Science and Technology (HUST), Wuhan, China in 2014 under the supervision of Professor Caihua Xiong. He is a member of IEEE and MIET member of the Institution of Engineering and Technology (IET).

Caihua Xiong (M'12) received the Ph.D. degree in mechanical engineering from Huazhong University of Science and Technology (HUST), Wuhan, China, in 1998. From 1999 to 2003, he was with the City University of Hong Kong and the Chinese University of Hong Kong, Hong Kong, as a Postdoctoral Fellow, and Worcester Polytechnic Institute, Worcester, MA, USA, as a Research Scientist. He has been a Chang Jiang Professor at HUST since 2008. His current research interests include biomechatronic prostheses, rehabilitation robotics, and robot motion planning and control. He is also the Director of the Institute of Rehabilitation and Medical Robotics at HUST.

Shigang Yue (M'05) received the Ph.D. degrees from Beijing University of Technology (BJUT), Beijing, China, in 1996. He is a Professor of Computer Science in the School of Computer Science, University of Lincoln, UK. He worked in BJUT as a Lecturer (1996-1998) and an Associate Professor (1998-1999). He was a Senior Research Assitant in MEEM, City University of Hong Kong (1998-1999). He was an Alexander von Humboldt Research Fellow (2000, 2001) at University of Kaiserslautern, Germany. Before joining the University of Lincoln as a Senior Lecturer (2007) and promoted to Reader (2010) and Professor (2012), he held research positions in the University of Cambridge, Newcastle University and the University College London (UCL) respectively. His research interests are mainly within the field of artificial intelligence, computer vision, robotics, brains and neuroscience. He is particularly interested in biological visual neural systems and their applications in unmanned ground/aerial vehicles, interactive systems and robotics. He is the founding director of Computational Intelligence Laboratory (CIL) in Lincoln and the deputy director of Lincoln Centre of Autonomous Systems (L-CAS). He is the coordinator for several EU FP7 and Horizon 2020 projects.